JTTEE5 13:396-404
DOI: 10.1361/10599630420443
1059-9630/$19.00 © ASM International

Peer Reviewed

Correlation Between Spraying Conditions and Microcrack Density and Their Influence on Thermal Cycling Life of Thermal Barrier Coatings

Robert Vaßen, Franziska Traeger, and Detlev Stöver

(Submitted August 30, 2003; in revised form November 3, 2003)

It is generally known that the porosity of thermal barrier coatings is essential to guarantee a sufficiently high strain tolerance of the coating during thermal cycling. However, much less is known about the influence of the specific morphology of porosity, such as microcracks and typically larger pores, on the performance of the coatings. Both features are usually formed during plasma spraying of yttria-stabilized zirconia (YSZ) thermal barrier coatings (TBCs). In this investigation, the influence of microcracks on the thermal cycling behavior was studied. The amount of microcracks within YSZ thermal barrier coatings was changed by changing the powder-feeding rate. Only small changes of the total porosity were observed. Mercury porosimetry served as a tool to investigate both the amount of microcracks and pores in the coating. Additionally, microcrack densities were determined from metallographical investigations. A linear dependence between the amount of fine pores determined by Hg porosimetry and the crack density was obtained for one set of coatings. Thermal cycling TBC specimens with different microcrack densities were produced and tested in a gas burner test facility. At high surface temperatures (above 1300 °C), failure occurred in the ceramic close to the surface. Under these conditions, the samples with increased horizontal microcrack densities showed a significant increase of thermal cycling life.

Keywords atmospheric plasma spraying, microcrack density, porosity levels, thermal barrier coatings, thermal cycling

1. Introduction

For more than 20 years, yttria-stabilized zirconia (YSZ) thermal barrier coatings (TBCs) have been developed for applications in gas turbines. An early investigation by Stecura[1] showed the influence of the yttria content and the porosity level on the thermal cycling performance of YSZ coatings. It turned out that an amount of 6-8 wt.% yttria and a porosity level of 14-15% performed best. Since this investigation, several papers have dealt with the influence of different structural characteristics on the thermal cycling behavior. It was found that segmentation cracks introduced into thick TBCs can improve the thermal cycling behavior.[2] The present investigation considers rather thin coatings with thicknesses below 0.5 mm that are typically used for applications on blades and vanes. The kind of damage after thermal cycling in such coatings depends on the thermal loading conditions and on the TBC system characteristics. For rather moderate loading conditions with surface temperatures below 1300 °C, it is often found that cracks develop close to the TBC and bondcoat interface.[3,4] Crack propagation is driven in this case by stresses, which develop due to the mismatch in thermal expansion coefficients during cooling and which are further enhanced by the growth of a thermally grown oxide (TGO) on the bondcoat. Typically, large parts of the coating spall off during this kind of failure.

A second type of failure is found at higher surface temperatures above 1300 °C and moderate bondcoat temperatures.[5] Especially close to the surface of the TBC, which is the region of highest temperatures, the ceramic starts to spall off lamella by lamella. The reason for this kind of failure is because the limit of temperature capability of YSZ is reached. Two mechanisms are responsible for this limited temperature capability, the enhanced sintering of the TBC[6] and phase transformations within the TBC.[7] The first mechanism, sintering, leads to an increase of the Young's modulus of the coating and a reduction of its strain tolerance. Both induce an increase of the stress level in the coating. The second mechanism, the phase transformation, is related to the nonequilibrium t'-phase typically present in plasma-sprayed YSZ coatings. Due to diffusion processes, this phase is not stable for long times at elevated temperatures. The t'-phase transforms into tetragonal and cubic phases. The tetragonal phase transforms then into the monoclinic phase during cooling. This process is accompanied by a large volume increase, which can promote spallation.

All failure mechanisms are affected by the microstructure of the coating. However, little has been published to date to the authors' knowledge on the influence of the microcrack density of the coating on its performance. For clarification, it should be mentioned that the term "microcracks" refers in this publication

Robert Vaßen, Franziska Traeger, and **Detlev Stöver,** Institut fuer Werkstoffe und Verfahren der Energietechnik 1, Forschungszentrum Jülich GmbH, Jülich, Germany. Contact e-mail: r.vassen@fz-juelich.de.

to the cracks perpendicular to the spray direction, which are sometimes termed horizontal microcracks.

Microcracks typically exist in plasma-sprayed ceramic coatings due to the fast cooling of the molten splats. This cooling process leads to tensile stresses in the sprayed lamellae. At a certain stress level, cracks form between the already sprayed layers and the freshly sprayed lamella (interlamellar cracks) and within freshly sprayed lamella (intralamellar cracks). The development of cracks, especially of vertical cracks, has been discussed in several papers.[8,9] Although there are a few contrary findings, it is believed that an increase in the substrate temperature promotes the formation of vertical cracks, while it reduces the probability of horizontal microcracks. In this study, a different approach using a variation of the feeding rate to adjust the horizontal microcrack density is discussed in more detail.

It has been stated that increased horizontal microcrack densities lead to reduced thermal shock life.[10] In the same investigation, however, the horizontal microcrack density has been mainly varied through the processing of different powders, which makes difficult the discrimination of the influence of only the microcrack density.

Porosity and both vertical and horizontal microcracks in TBCs are key parameters that give the coatings its strain tolerance due to both reduced Young's modulus and hence low stress values[11] and due to stress relaxation.[12] Without those features, the ceramic coating system would hardly be able to withstand the stress levels arising during thermal cycling. The focus of the present investigation is on the influence of the microcrack density on the high-temperature failure mode of the YSZ TBCs. It is found that the detrimental effects especially of the sintering can be significantly influenced especially by the amount of horizontal microcracks within the coating structure.

2. Experimental

2.1 Samples

The investigated thermal barrier coating systems have been produced by plasma spraying with Sulzer Metco plasma-spray units (Sulzer Metco AG, Wohlen, Switzerland). The YSZ powder was a 7.8 wt.% yttria-stabilized zirconia powder (Metco 204 NS) supplied by Sulzer Metco, Hattersheim, Germany. Plasma spraying under a low pressure of neutral atmosphere (i.e., VPS) with a F4 gun was used to deposit a 150 μm NiCoCrAlY bondcoat (Ni 192-8 powder by Praxair Surface Technologies Inc., Biebesheim, Germany) on disk-shaped nickel-based IN738 superalloy substrates, which were used for thermal cycling experiments. The substrates used had a diameter of 30 mm and a thickness of 3 mm. The outer edge exhibited a curvature radius of 1.5 mm. This geometry was chosen to minimize the effect of stresses originating at the specimen free edges.[13] The ceramic top coats with a thickness between 225 and 440 μm were produced by atmospheric plasma spraying (APS) using a Triplex gun.

2.2 Processing Parameters

The argon and helium plasma gas flow rates during spraying were 20 and 13 standard liters per minute (slpm), respectively. The plasma current was 300 A, the carrier gas flow was 1.5 slpm of Ar. The feeding rate was varied between 2.5% and 30%, which corresponded to about 4.4-54.7 g/min. The spray gun was mounted on a six-axis robot, which moved at a speed of 500 mm/s. Two sets of coatings have been produced with these process conditions. The spraying of set 1 was made with a rather old set of cathodes, while for set 2 new cathodes were used. This led to the fact that the first set was produced with an electrical torch power of 20.9 kW, while the second set was produced with a higher torch power of between 22.9 and 23.6 kW (Table 1).

Table 1 Description of the Investigated Coatings

Set	Feeding Rate, g/min	Gun Power, kW	Number of Passes	Coating Thickness, μm	Layer Thickness Per Pass, μm
1	9.1	20.9	50	360	7.2
	18.2	20.9	25	400	116.0
	36.4	20.9	12	~350	~29
2(a)	4.4	23.0/23.6	95/120	285/365	3.0/3.0/2.9
	9.1	22.9/23.0	34/60	225/375	6.3/6.6
	36.4	22.9/23.1	12/20	320/460	23.0/26.7
	54.7	22.8/23.0	8/15	260/450	30.0/32.5

(a) In set 2, the first sample of each feed rate condition was used for thermal cycling, while the second was used for Hg porosimetry.

2.3 Thermal Cycling

Thermal cycling was performed in two gas burner test facilities operating with natural gas and oxygen. The substrates were cooled by compressed air from the back. The surface temperature was measured with a pyrometer operating at a wavelength range of 8-11.5 μm and a spot size of 12 mm. The emissivity of YSZ at this wavelength range was determined to be close to 1.[14] Additionally, the substrate temperature was measured by a thermocouple mounted in a hole drilled 15 mm toward the center of the substrate from one side. The surface temperature was varied between about 1320 and 1360 °C, the substrate temperature was adjusted between 990 and 1040 °C. Using the average thermal conductivities of the coatings and the substrate (about 1 W/m/K[15] and about 27 W/m/K[16], respectively), one can estimate that the bondcoat temperature is about 30-55 K higher than the substrate temperature. Therefore, the bondcoat temperatures were in the range between 1045 and 1095 °C.

In the test facilities, gas burners with a broad flame were used giving a fairly homogeneous temperature distribution in the center of the samples. After heating for about 20 s, the maximum temperature is nearly reached. After 5 min the burner is automatically removed for 2 min from the surface, and the surface is cooled from the front at an initial rate of more than 100 K/s using compressed air.

Cycling was stopped when a clearly visible peeling of the coating on a length of 5 mm occurred. However, the specimens are not inspected after each cycle and the installed automatic system can only detect spallation if a rather large temperature change occurs at the surface of the coating. As a result, a certain number of cycles can be performed even after spallation, which gives a certain uncertainty in the number of cycles typically below 20% of the total cycle number.

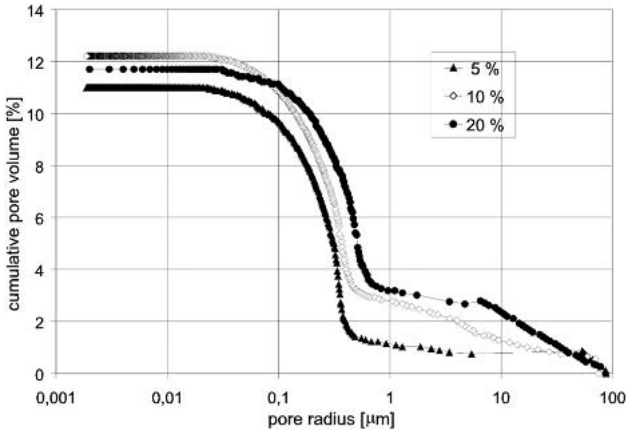

Fig. 1 Mercury porosimetry measurements for coatings sprayed with three different feeding rates, i.e., 9.1, 18.2, and 36.4 g/min

2.4 Pore Level Quantification

Besides the manufacture of the thermal cycling specimens, steel substrates were also coated. These coatings were used to characterize the as-sprayed condition. The porosity level was measured on freestanding coatings by mercury porosimetry using two units of porosimeters produced by CE Instruments, Italy (types: Pascal 140 for the low-pressure range 0.01-400 kPa above atmospheric pressure as well as Pascal 440 for the high-pressure range up to 400 MPa; CE Instruments, marketed by Porotec GmbH, Frankfurt am Main, Germany). Coatings were removed from the substrates by dissolving them in hydrochloric acid.

Metallographic sections were prepared from all samples to investigate the microstructure. The coatings were embedded with epoxy before cutting to reduce the possibility of damage. Microcrack densities have been determined by counting the number of cracks that intersect a line drawn through the coating in the spray direction and dividing this number by the length of the line. Analysis was made on images of an optical microscope, which allowed a resolution of about 500 nm. With this procedure only horizontal microcracks were measured. Five measurements have been made for each type of coatings and the results were averaged.

3. Results and Discussion

3.1 Microstructural Investigations

The results of Hg porosimetry measurements are shown in Fig. 1. The total porosity of all coatings is similar (11-12%). However, there is a distinct difference in the amount of fine pores below 1 µm, i.e., the step height of the fine part of the distribution, which is attributed to microcracks.[17] Micrographs of the coatings are shown in Fig. 2, where no large difference in the microstructure appears at the given magnification. However, a determination of the microcrack density revealed a clear reduction with increasing the feeding rate. In Fig. 3, the fraction of fine pores as a function of the crack density is plotted for the first set of experiments. Obviously, a linear dependence between the fine pore fraction and the microcrack density exists, indicating that the fine pores in the Hg porosity measurements can be, at least partly, attributed to microcracks. However, the linear line fitting the three data points intersects the axis of the pore fraction at 6% and not at 0%. An explanation of this behavior is the fact that vertical microcracks are present in the coating and are not resolved on the optical micrographs and hence not measured with the intersect method. In addition, it is also assumed that a certain amount of fine pores determined by Hg porosimetry has to be attributed to larger pores, which have been filled through smaller pores. With increasing coating thickness, the amount of large pores measured as fine porosity is expected to increase. As a result, a precise determination of the influence of process parameters on microcracks with Hg porosity is only possible if coatings with similar thickness are used for the measurements. This requirement was sufficiently fulfilled only for set 1.

For the second set of coatings, measurements of porosity and microcrack density have been also performed. It turned out that the observed microcrack densities were close to the ones observed for the first set of coatings (Fig. 4). For the investigated coatings, a reduction of the microcrack density measured with the intersect method is observed with increasing the feeding rate. The slight increase of the crack density for the highest feeding rate might be due to the fact that a regime in which not all powder particles can be completely molten is approached.

In contrast to the results for the first set of coatings, an increase of the fraction of fine pores with crack density for the coatings cannot be observed. The reasons are not fully clear; however, it is assumed that larger variations of thickness gave a larger scatter in the Hg porosimetry data. In particular, the two coatings with high segmentation crack densities show low fractions of fine pores. This is consistent with the fact that the thickness is lower for these coatings, and, as discussed above, the contribution of large pores measured as fine pores is relatively low.

The total porosity of the coatings, which should be correct despite of different coating thicknesses, were in the range of 12-13% for feeding rates between 9.1 and 54.7 g/min. Only the coatings produced with 4.4 g/min feeding rate showed a significantly higher porosity level of about 15%. Micrographs of the coatings of set 2 are shown in Fig. 5.

In the following, a qualitative understanding of the described phenomena is proposed.

First estimate the time that a deposited particle needs to cool down to about half of the difference between melting (2680 °C) and coating (about 200 °C) temperature, that is to say 1240 °C. It is assumed that the incoming particle is at melting temperature and the coating temperature stays constant during cooling. Two major contributions, the heat of fusion (ΔH_f about 7×10^5 J/kg[18]) and the heat ΔH_{cp} due to the specific heat of the spray lamellae (c_p about 0.6 J/K · g[19]), are considered to be transferred to the substrate. The heat flux through the lamella is approximated by Fick's first law[20] assuming that the temperature gradient across the spray lamellae, defined by the difference of melting temperature T_m and substrate temperature T_{sub} divided by the lamella thickness l, is expressed as follows:

$$[\Delta H_f + \Delta H_{cp}]\rho l = \lambda \frac{T_m - T_{sub}}{l} t \quad \text{(Eq 1)}$$

where ρ is the density (6 g/m[21]), λ the thermal conductivity (2 W/m/K[21]) and l the thickness of the sprayed YSZ lamella.

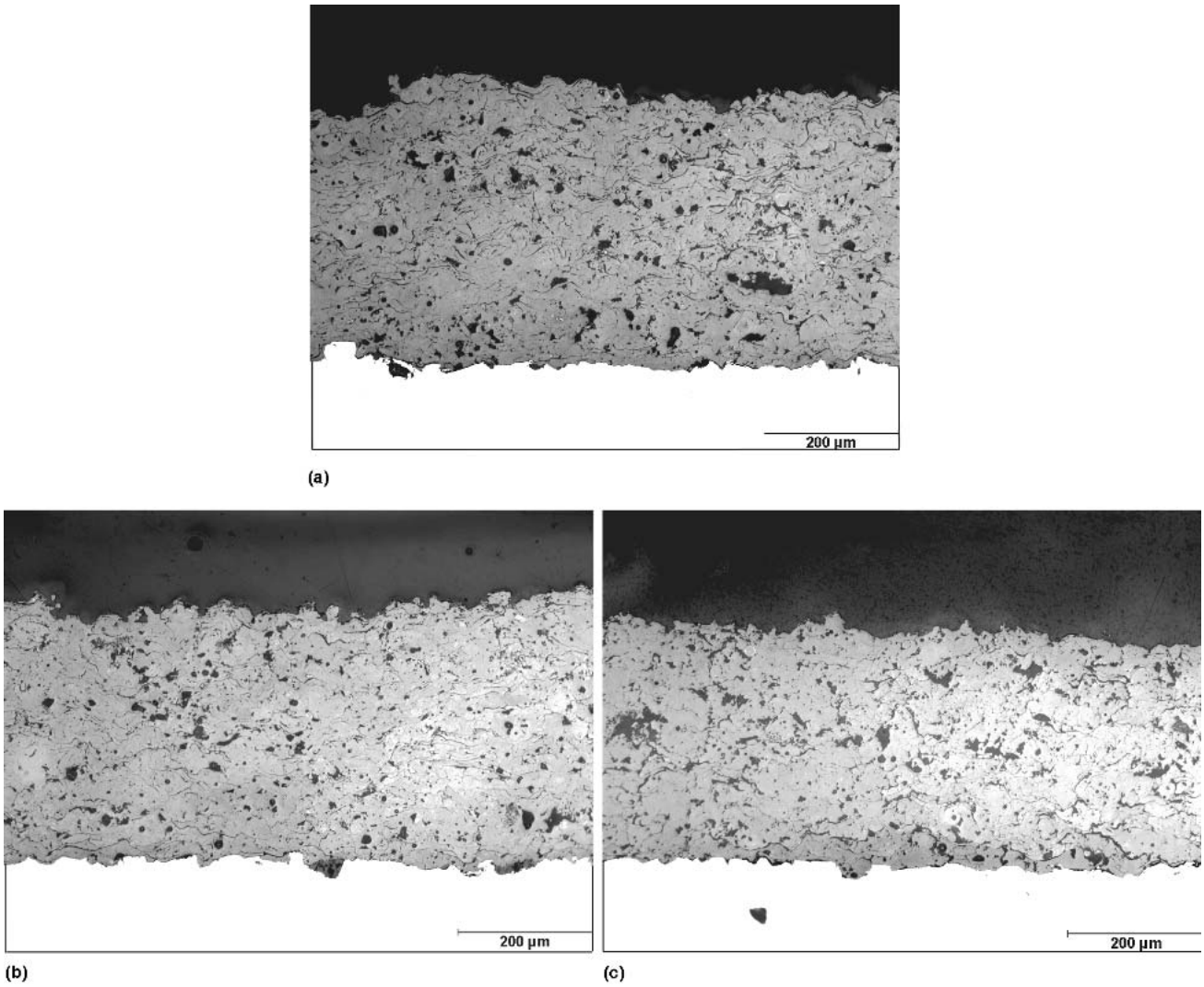

Fig. 2 Micrographs of coatings sprayed with **(a)** 9.1, **(b)** 18.2, and **(c)** 36.4 g/min feeding rates

Hence, the time t after which the lamella has cooled down to half the melting temperature (m) can be estimated as follows:

$$t = \frac{\Delta H_f + c_p \frac{(T_m - T_{sub})}{2}}{T_m - T_{sub}} \frac{\rho l^2}{\lambda} \quad \text{(Eq 2)}$$

For the given input parameters and a lamella thickness of about 7 µm, a time of 0.1 ms is calculated. The lamella thickness was estimated from scanning electron microscope pictures of fracture surfaces (Fig. 6). In this simple model, the free surface of the lamella is, after this time, still at the melting temperature. The cooling via radiation is neglected as it is estimated to be about a factor of 100 smaller than the one via thermal conduction. During further cooling, the gradient will be reduced both due to the decrease of the lamella temperature and the increase of the substrate temperature. Hence, cooling will slow down, and it is expected that after 1 ms the free surface of the lamella still has a temperature well above the substrate temperature.

Now consider the deposition process. The robot with the spray gun moves at a velocity v of 500 mm/s. The particle flux footprint d ahead of the plasma gun was on the order of about 5 mm. Therefore the time t_{dep} during which particles can be deposited on a certain point of the substrate during one pass corresponds to:

$$t_{dep} = d/v = 10 \text{ ms} \quad \text{(Eq 3)}$$

If the thickness deposited during one pass is now considered (Table 1), it is found that for feeding rates larger than 9.1 g/min the thickness per pass is larger than the lamella thickness of about 7 µm. Hence, several particles are deposited during one pass. As discussed previously, all these particles are probably still rather hot and so the cooling to substrate temperatures leads to reduced tensile strain differences between adjacent lamellae. In Fig. 7, this mechanism is schematically illustrated.

As a result, the probability of microcrack formation is reduced for higher feeding rates. This could explain the results found in these experiments (Fig. 4).

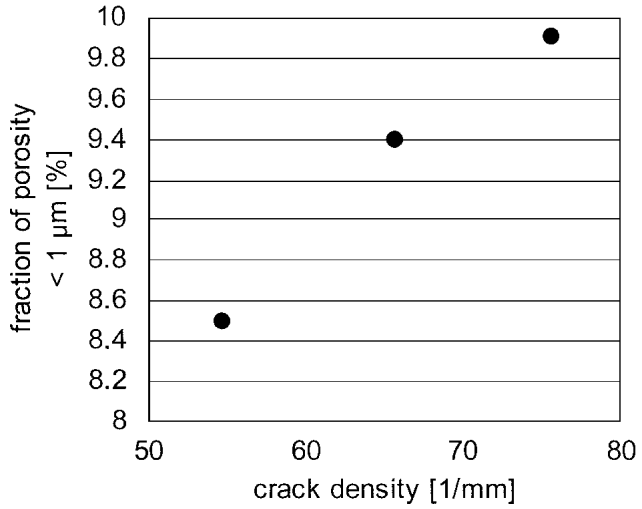

Fig. 3 Fraction of pores below 1 µm of characteristic dimension as a function of microcrack density for set 1 of coatings

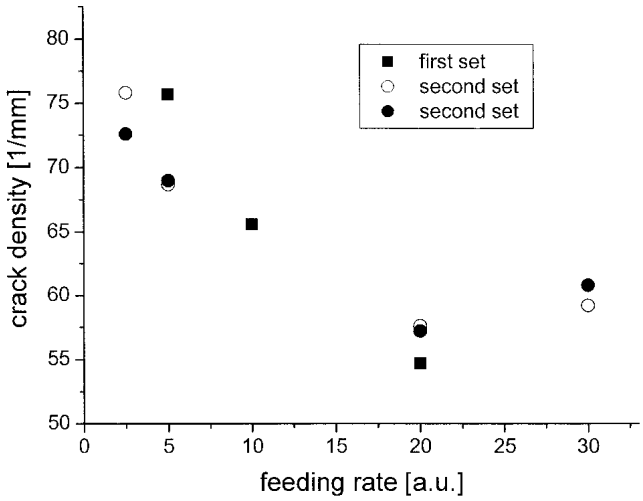

Fig. 4 Microcrack density as a function of feeding rate for set 1 (squares) and set 2 of coatings (circles, measurements on both types of samples given in Table 1 have been performed)

3.2 Thermal Cycling

Figure 8 displays the number of cycles to failure as a function of the surface temperature. The surface temperature was calculated as a mean value over all heating cycles, taking into account only the last 4 min of the 5 min heating period. The surface temperatures showed considerable variations. The cycle numbers showed also a relatively large variation even for equal feeding rates. However, certain tendencies are visible as indicated by the linear correlations, which are obtained by visual approach. These lines were plotted to take into account the fact that large standard deviations will shift the actual surface temperatures to considerably higher temperatures. Obviously, the lifetime at temperatures above 1350 °C is low for all systems. For temperatures between 1320 and 1350 °C, however, longer lifetimes are observed. The data indicate in this temperature range increasing cycle numbers till failure with decreasing feeding rate. This statement is supported by the shown linear correlations, which give the approximate dependence of cycles to failure as a function of surface temperature for the different feeding rates.

For a more detailed analysis of the occurring phenomena the kind of failure was examined. Most of the samples showed spalled regions at the surface of the ceramic. This kind of failure was observed earlier[5] and can be attributed to the limited temperature capability of YSZ coatings. This is proved by a microstructural examination of the coatings. As an example, the microstructure of a coating with large feeding rate (36.4 g/min) after thermal cycling is shown in Fig. 9(a). Large cracks within the coating, mainly horizontally oriented, are found. These cracks, especially at the free surface near regions of the TBC, indicate the failure. A more microstructural-based explanation of the failure is discussed thereafter.

For two thermal cycling samples (Fig. 10a and b), both produced with low feeding rates, part of the coatings spalled off at the outer rim or the center. This kind of failure is typically due to the growth of the TGO and not due to the limited temperature capability of the coatings, which is underlined by a microstructural characterization of the TBC systems. In Fig. 9(c), the microstructure of a coating prepared with 4.4 g/min feeding rate is shown. The long cracks close to the ceramic/bondcoat and the thermally grown oxide are clearly visible.

The given differences in failure modes between samples with low and high feeding rates are also observed for samples after cycling (Fig. 10). The parameters of thermal cycling at relatively low temperatures (below 1350 °C) for these four samples with different feeding rates cycled are given in Table 2.

For surface temperatures close to or higher than 1350 °C, the differences between the type of failure for samples elaborated with low and high feeding rate vanishes (Fig. 9b and d).

A qualitative understanding of the high-temperature failure of the coatings is now proposed.

As mentioned previously, two mechanisms are predominantly responsible for the failure of the YSZ coatings at high temperatures: sintering and phase transitions. First consider the effect of sintering in combination with stress relaxation within the TBC. It is assumed that the most important effect of sintering is the increase of Young's modulus. As this effect is strongly related to the temperature, the modulus increases from the bondcoat to the top of the TBC after thermal cycling. In addition, stress relaxation is faster at the surface of the TBC. Stresses build up as the thermal expansion coefficient of the substrate and the bondcoat are larger than the one of the TBC. Starting from a nearly stress-free system at room temperature, in-plane tensile stresses develop in the TBC at elevated temperatures. These stresses are reduced by the stress relaxation. As known from previous calculations, stress relaxation is quite fast.[4] So, for simplification, it is assumed that the stress in the whole TBC is close to zero at high temperatures after a limited number of cycles. Cooling down the system to room temperature develops compressive stresses in the coating. The compressive stress levels can be determined from the product of strain and Young's modulus of the coating. As the surface is at a higher temperature, the compressive strain is reduced at this location after cooling to room temperature. However, this effect is overcompensated by the larger increase of Young's modulus at the surface compared

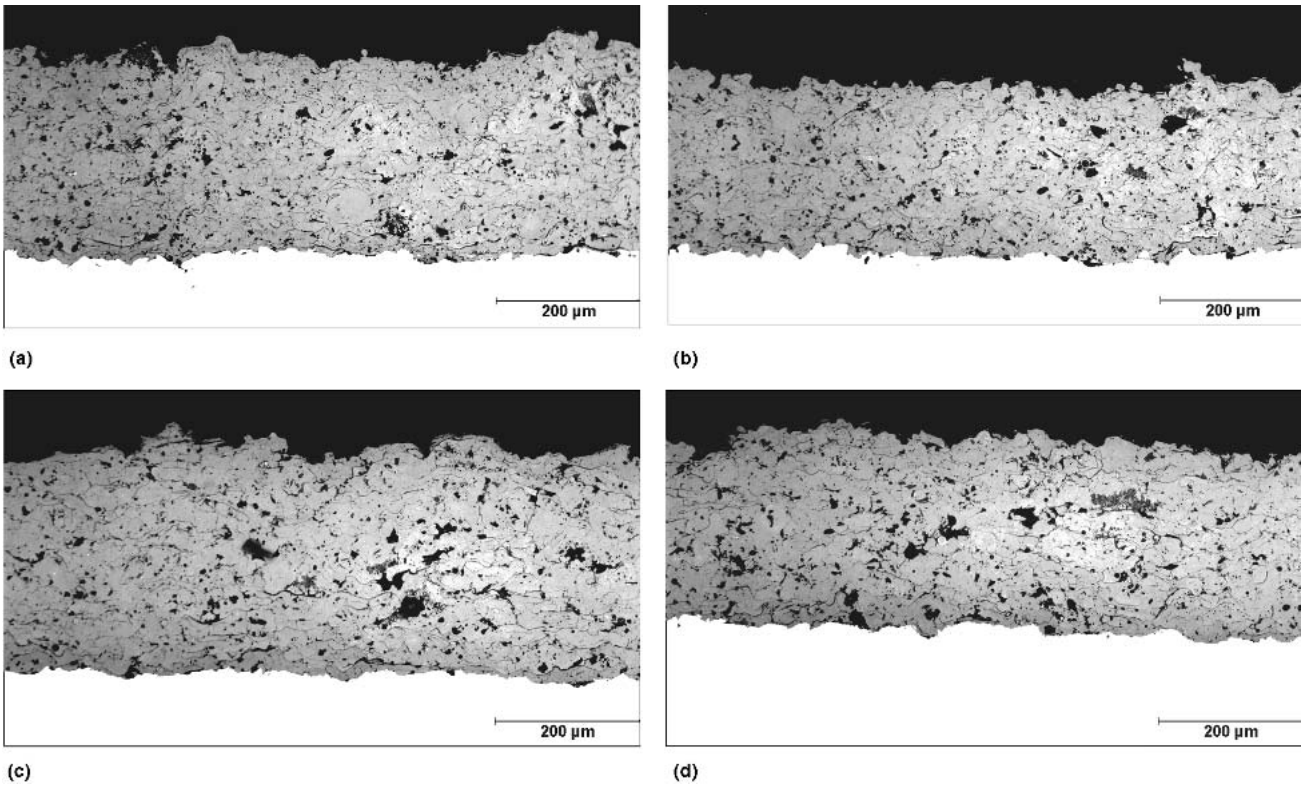

Fig. 5 Coatings for set 2 sprayed with different feeding rates [from (a-d) to 4.4, 9.1, 36.4, and 54.7 g/min]

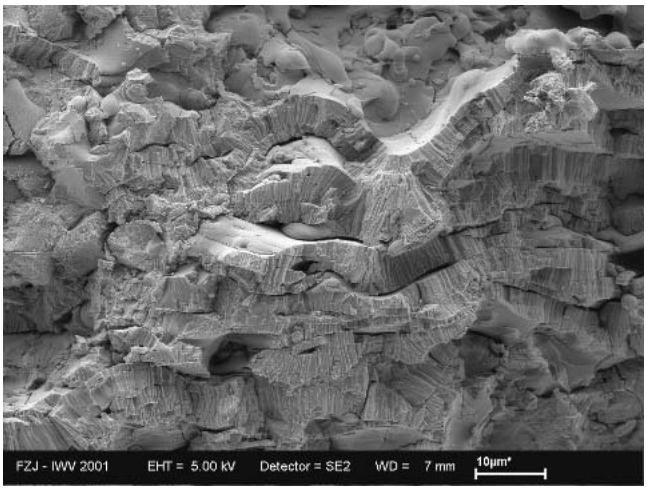

Fig. 6 Surface fracture of a thermal barrier coating sprayed with a feeding rate of 9.1 g/min (SEM view)

with the regions close to the bondcoat. As a result, the compressive stress levels will increase throughout the coating toward the surface.

Stress gradient through the TBC is also present within the part of the coating deposited during one path of the spray gun. This part will be denoted as "layer" in the following. As discussed previously, the layer can consist of several individual single-spray lamellae and probably microcracks are formed at

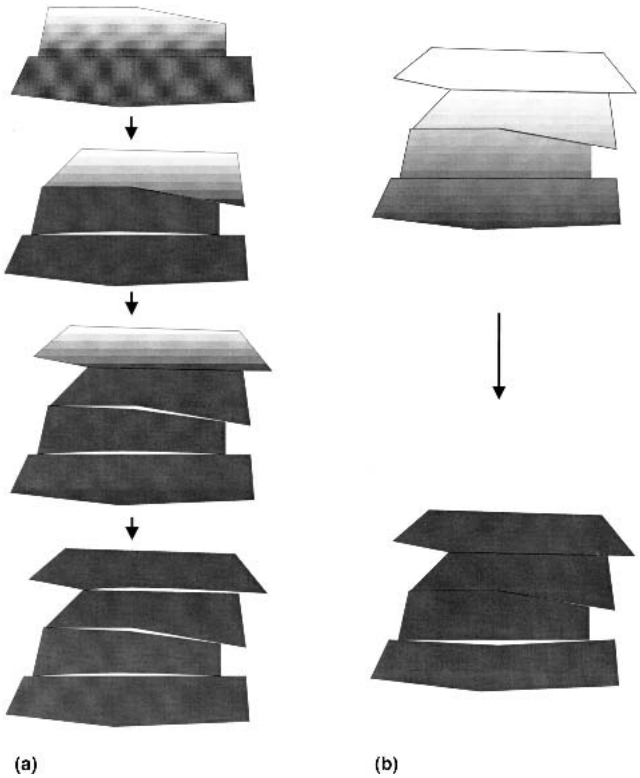

Fig. 7 Schematic showing the formation of microcracks during the deposition and cooling of splats using **(a)** low and **(b)** high feeding rate

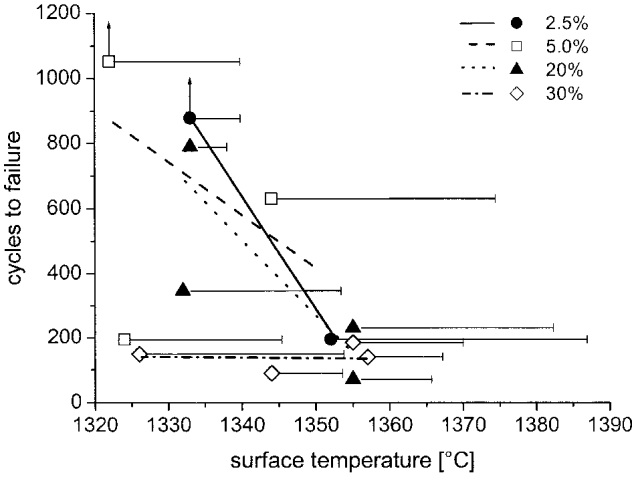

Fig. 8 Number of cycles to failure for coatings produced with different feeding rates as a function of the surface temperature. The arrows indicate a failure at the bondcoat. The error bars indicate the standard deviation of the surface temperatures.

the contact surface to the next layer. This stress gradient leads to a bending momentum through this layer in combination with tensile stress perpendicular to the horizontal microcracks (Fig. 11). As the stress level increases beyond a critical value, it can finally lead to a spallation of the layers, as observed in the experiments. The magnitude of the tensile stresses should increase with the stiffness and the thickness of the layers. From elastic thin plate theory, one can estimate these stresses to be proportional to the cube of the ratio of height to length of the layers.[22] For a height of 20 μm, which is slightly lower than the typical pass thickness for a feeding rate of 36.4 g/min (Table 1), a length of 100 μm and an elastic modulus change of 1 GPa through the layer will result in a tensile stress level at the interface in the MPa range. This value indicates that the given explanation is a possible mechanism of surface spallation. In addition, it is able to explain the influence of microcrack densities on the thermal cycle life of the coatings.

At further higher temperatures, it is possible that the second mechanism, that is, the phase transformation from t' to tetragonal and cubic (and further to monoclinic and cubic during

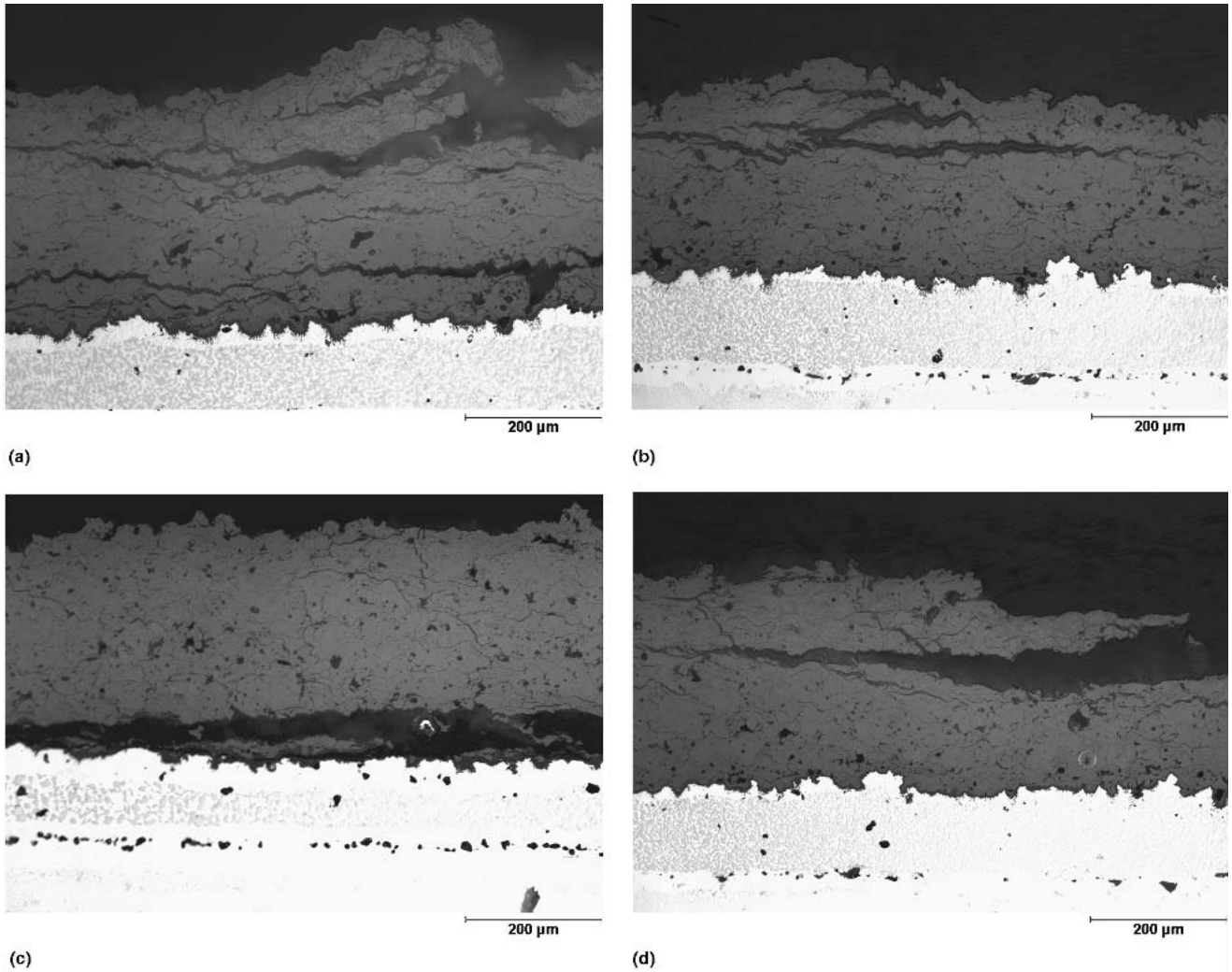

Fig. 9 Microstructure of specimens produced with "high" (36.4 and 54.7 g/min) feeding rates **(a)** cycled at T_{surf} = 1333 °C for 790 cycles, **(b)** cycled at T_{surf} = 1355 °C for 185 cycles and "low" (9.1 g/min) feeding rate, **(c)** cycled at T_{surf} = 1333 °C for 878 cycles, and **(d)** cycled at T_{surf} = 1352 °C for 195 cycles

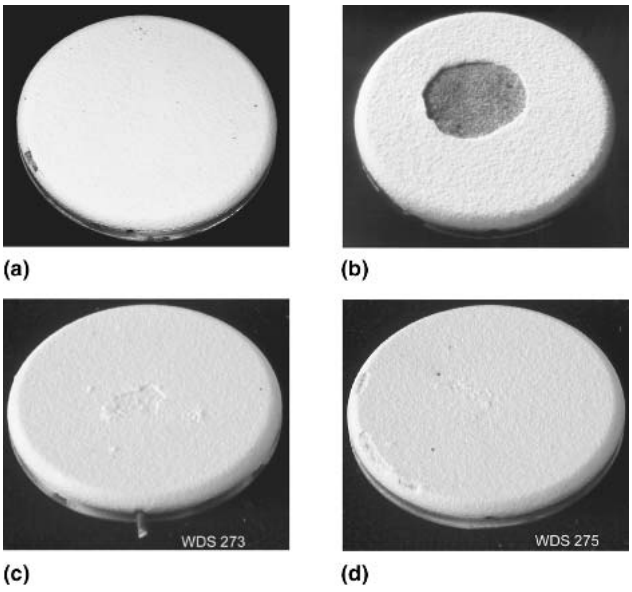

Fig. 10 Samples after thermal cycling. The parameters are listed in Table 2; the feeding rates increased from **(a)** to **(d)**.

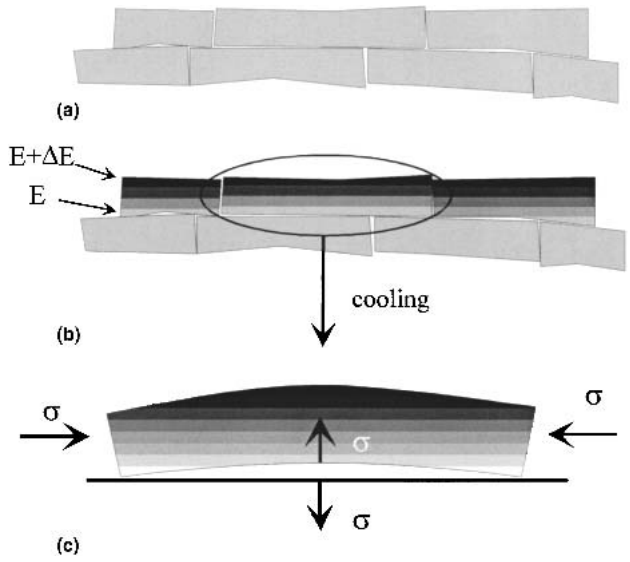

Fig. 11 Schematic showing the buildup of stresses in the lamella during cooling: **(a)** as-sprayed coating, **(b)** coating after sintering (only shown for top layer), and **(c)** stress buildup during cooling in one layer. The dark color indicates higher Young's modulus.

Table 2 Parameters of Some Thermally Cycled Specimens Corresponding to Set 2

Feeding Rate, g/min	$T_{surface}$, °C	$T_{bondcoat}$, °C	Number of Cycles	Location of Failure
4.4	1333	1067	878	Outer rim, interface TBC/bondcoat
9.1	1322	1047	1052	Center, interface TBC/bondcoat
36.4	1333	1064	790	In ceramic
54.7	1326	1074	149	In ceramic

cooling), which is accompanied by a large volume change, is becoming increasingly important. It is probable that the introduced stresses cannot be compensated by the strain tolerant microcracked structure or the material already has lost this property due to sintering effects.

As a result, microcrack densities do not significantly improve the performance at these extremely high surface temperatures. For this temperature regime, new materials and concepts, as described for example in Ref 23, are needed.

4. Summary

In the current study, it was shown that high microcrack densities in TBCs can be adjusted by the use of low feeding rates. Besides metallographical examinations, mercury porosimetry was also used to characterize the microcracks. However, certain requirements have to be fulfilled to obtain reliable results from the mercury intrusion technique, such as well-defined coating thickness. A simple model was presented to explain the correlations between the feeding rate value and the microcrack density.

In a second time, the influence of the microcrack density on the thermal cycling performance in a gas burner test facility was studied. It turned out that in the surface temperature range between 1320 and 1350 °C, the samples with high microcrack densities showed an improved performance. A mechanism was suggested and related to the observed spallation, lamella by lamella, starting from the surface of the TBC. A key parameter in this case is the temperature gradient, which leads to a different amount of sintering and hence different elastic moduli throughout the coating thickness. As a result, bending moments are present within individual spray lamella that induce their spallation. The improved performance of coatings sprayed with low feeding rates can hence be understood with this model.

Acknowledgments

The authors would like to thank Mr. K.-H. Rauwald and Mr. R. Laufs (both IWV1, FZ Jülich) for the manufacturing of the plasma-sprayed coatings and the thermal cycling of the specimens. The authors also gratefully acknowledge the work of Mrs. S. Schwartz-Lückge and Mr. M. Kappertz (both IWV1, FZ Jülich) who performed the characterization of the specimens.

References

1. S. Stecura: "Optimization of the Ni-Cr-Al-Y/ZrO_2-Y_2O_3 Thermal Barrier System," *Adv. Ceram. Mater.,* 1986, *1*(1), pp. 68-76.
2. P. Bengtsson, T. Ericsson, and J. Wigren: "Thermal Shock Testing of Burner Cans Coated with a Thick Thermal Barrier Coating," *J. Therm. Spray Technol.,* 1998, *7*(3), pp. 340-48.
3. Z.Z. Mutasim and Y.L. Nava: "Development and Performance of Thick Air Plasma Sprayed Thermal Barrier Coatings," in *Thermal Spray: Surface Engineering via Applied Research,* C.C. Berndt, ed., ASM International, Materials Park, OH, 2000, pp. 1325-30.
4. R. Vaßen, G. Kerkhoff, and D. Stöver: "Development of a Micromechanical Life Prediction Model for Plasma Sprayed Thermal Barrier Coatings," *Mater. Sci. Eng.,* 2001, *A*303(1-2), pp. 100-09.
5. R. Vaßen, G. Barbezat, and D. Stöver: "Comparison of Thermal Cycling Life of YSZ and $La_2Zr_2O_7$-Based Thermal Barrier Coatings," in *Mate-*

rials for Advanced Power Engineering 2002, J. Lecomte-Becker, M. Carton, F. Schubert, and P.J. Ennis, ed., Schriften des Forschungszentrum Jülich, Reihe Energietechnik, Jülich, Germany, Vol. 21, Part 1, 2002, pp. 511-21.
6. R. Vaßen, N. Czech, W. Malléner, W. Stamm, and D. Stöver: "Influence of Impurity Content and Porosity of Plasma Sprayed Yttria Stabilised Zirconia Layers on the Sintering Behaviour," *Surf. Coat. Technol.,* 2001, *141,* pp. 135-40.
7. R.A. Miller, J.L Smialek, and R.G. Garlick: "Phase Stability in Plasma-Sprayed Partially Stabilized Zirconia-Yttria," in *Science and Technology of Zirconia*, *Advances in Ceramics,* Vol. 3, A.H. Heuer and L.W. Hobbs, ed., The American Ceramic Society, Columbus, OH, 1981, pp. 241-51.
8. P. Bengston and T. Johannesson: "Characterization of Microstructural Defects in Plasma-Sprayed Thermal Barrier Coatings," *J. Therm. Spray Technol.,* 1995, *4*(3), pp. 245-51.
9. P. Bengston and J. Wigren: "Segmentation Cracks in Plasma-Sprayed Thick Thermal Barrier Coatings," in *Gas Turbine Materials Technology,* P.J. Maziasz and I.G. Wright, ed., ASM International, Materials Park, OH, 1999, pp. 92-101.
10. J. Wigren, J.-F. de Vries, and D. Greving: "Effects of Powder Morphology, Microstructure, and Residual Stresses on Thermal Barrier Coating Thermal Shock Performance," in *Thermal Spray: Practical Solutions for Engineering Problems,* C.C. Berndt, ed., ASM International, Materials Park, OH, 1996, pp. 855-61.
11. J.A. Thompson and T.W. Clyne: "The Effect of Heat Treatment on the Stiffness of Zirconia Top Coats in Plasma-Sprayed TBCs," *Acta. Mater.,* 2001, *49,* pp. 1565-75.
12. M. Ahrens, S. Lampenscherf, R. Vaßen, and D. Stöver: "Sintering and Creep Processes in Plasma-Sprayed Thermal Barrier Coatings," *J. Therm. Spray Technol.,* 2004, *13*(3), pp. 433-43.
13. C. Funke, J.C. Mailand, B. Siebert, R. Vaßen, and D. Stöver: "Characterisation of ZrO_2-7 wt.% Y_2O_3 Thermal Barrier Coatings with Different Porosities and FEM Analysis of Stress Redistribution During Thermal Cycling of TBC's," *Surf. Coat. Technol.,* 1997, *94-95,* pp. 106-11.
14. J.I. Eldridge, C.M. Spuckler, K.W. Street, and J.R. Markham: "Infrared Radiative Properties of Yttria Stabilized Zirconia Thermal Barrier Coatings," *Ceram. Eng. Sci. Proc.,* 2002, *23*(4), pp. 417-30.
15. R. Dutton, R. Wheeler, K.S. Ravichandran, and K. An: "Effect of Heat Treatment on the Thermal Conductivity of Plasma-Sprayed Thermal Barrier Coatings," *J. Therm. Spray Technol.,* 2000, *9*(2), pp. 204-09.
16. F. Tomoharu and T. Takeshi: "Estimation of Thermophysical Properties of Coating Layers for Gas Turbine Hot Parts. Part1: Measurement of Thermophysical Properties of Coating Layers and Superalloys, and Comparison Between Virgin and Aged Material," *Denryoku Chuo Kenkyujo Yokosuka Kenkyujo Hohoku,* 1998, no. W97017, p. 20.
17. B. Siebert, C. Funke, R. Vaßen, and D. Stöver: "Changes in Porosity and Young's Modulus Due to Sintering of Plasma Sprayed Thermal Barrier Coatings," *J. Mater. Proc. Technol.,* 1999, *92-93,* pp. 217-23.
18. I. Ahmed and T.L. Bergman: "Three-Dimensional Simulation of Thermal Plasma Spraying of Partially Molten Ceramic Agglomerates," *J. Therm. Spray Technol.,* 2000, *9*(2), pp. 215-24.
19. S. Raghavan, H. Wang, R.B. Dinwiddie, W.D. Porter, and M.J. Mayo: "The Effect of Grain Size, Porosity and Yttria Content on the Thermal Conductivity of Nanocrystalline Zirconia," *Scri. Mater.,* 1998, *39*(8), pp. 1119-25.
20. J. Crank: *The Mathematics of Diffusion,* Clarendon Press, Oxford, UK, 1975, p. 2.
21. R. Morrell: *Handbook of Properties of Technical & Engineering Ceramics,* Part 1, HMSO Publications, London, UK, 1989.
22. I. Szabo: *Höhere Technische Mechanik,* Springer Verlag, Berlin, Germany, 2001, p. 192.
23. R. Vaßen, X. Cao, and D. Stöver: "Improvement of New Thermal Barrier Coating Systems Using a Layered or Graded Structure," *Ceram. Eng. Sci. Proc.,* 2001, *22*(4), pp. 435-42.